Phosphorylation of the α subunit inhibits proteasome assembly and regulates cell division in archaea

Qihong Huang[*, †], Ya Wu[†], Qi Gan, Shikuan Liang, Yunfeng Yang, Pengju Wu, Xu Feng, Qunxin She, Jinfeng Ni, Yulong Shen[*]

CRISPR and Archaea Biology Research Center, State Key Laboratory of Microbial Technology, Microbial Technology Institute, Shandong University, 266237, Qingdao, China

[†]These authors contributed equally to this work: Qihong Huang, Ya Wu.

[*]Correspondence: yulgshen@sdu.edu.cn, huangqihong@sdu.edu.cn

Abstract

The archaea of the order Sulfolobales display a eukaryotic-like cell cycle. Here, we demonstrate that phosphorylation of the α subunit by a eukaryotic-like protein kinase ePK2 affects 26S proteasome assembly and controls cell division in *Saccharolobus islandicus*. ePK2 exhibits cell cycle-dependent expression at both transcriptional and translational levels. Deletion or overexpression of *ePK*2 results in impaired cytokinesis, with the deletion cells being unable to generate single chromosome cells after synchronization and the overexpression cells exhibiting growth retardation and cell enlargement. Interestingly, overexpression of ePK2 leads to a coherent reduction in cellular proteasome activity and degradation of cell division proteins. We identify S200 and T213 of the proteasome α subunit as specific target sites for ePK2 phosphorylation. Functional and structural analyses of site-directed mutants at S200 and T213 suggest that S200 phosphorylation disrupts the assembly of 20S into 26S proteasome whereas T213 phosphorylation interferes the *de novo* α ring assembly. Collectively, our study uncovers an ingenious and efficient mechanism of proteasome phosphorylation-mediated cell division regulation, a prototype of the eukaryotic cell cycle regulation system, in Sulfolobales archaea.

Key words

Archaea, Sulfolobales, cell cycle regulation, eukaryotic protein kinase (ePK), cell division, proteasome, protein phosphorylation

Introduction

The eukaryotic cell cycle consists of four main phases, G1 (the first gap), S (DNA synthesis), G2 (the second gap), and M (mitosis) phases[1]. The cell cycle is strictly regulated by a combination of cyclins and cyclin-dependent kinases (CDKs)[1-3]. Accumulation of specific cyclins during different cell cycle stages is accomplished by cell cycle-dependent transcription and inhibition of proteasome-mediated degradation. In turn, this transcription is dependent on CDK-mediated phosphorylation and activation[4,5]. The proteasomes are regulated by phosphorylation on multiple subunits of both 19S (Rpt3, Rpt5, Rpt6, Rpn6 and Rpn10) and 20S (α5 and α7) proteasome particles. Several studies have shown that phosphorylation of the proteasome subunits can either inhibit or stimulate the proteasome's degradation activity on cell cycle related proteins, thereby affecting cell proliferation[6-9]. Given the complexity of eukaryotic cell cycle regulation network[10-12], the detailed regulation of cell cycle and its origin remain a mystery.

TACK superphylum in archaea is phylogenetically close to eukaryotes[13-15]. The archaea of the order Sulfolobales within the Crenarchaeota phylum exhibit a eukaryotic-like cell cycle which contains G1, S, G2, M, and D (cell division) phases, accounting for < 5%, approximately 30%, > 50%, < 5%, and < 5% of the whole cell cycle, respectively. The cell division machinery in Sulfolobales resembles that of eukaryotes, encompassing several ESCRT-III (endosomal sorting complex required for transport III) homologs (also called CdvBs), Vps4 ATPase (or CdvC), and an archaeal-specific protein CdvA[16-19]. As other archaea, the information processing machineries of Sulfolobales are similar to those in eukaryotes[20-25]. Moreover, studies have revealed that Sulfolobales harbor a high-order level of chromosome organization

in the form of A and B compartments, indicating a prototypical chromosome architecture of eukaryotes[26,27]. Therefore, Sulfolobales are excellent models for investigating the mechanisms and origins of eukaryotic-like cell cycle processes and their regulation. Investigation in *Sulfolobus acidocaldarius* revealed that the proteasome initiates cell cytokinesis by degrading the cell division protein CdvB during the cell cycle[28]. We and others have shown that the cell division in *Saccharolobus islandicus* is dictated by a transcription factor called aCcr1. The protein binds to the promoters of dozens of genes including *cdvA* and represses their transcription[29,30]. However, many aspects of these processes remain largely unexplored.

Proteasome is highly conserved in archaea[31]. Sulfolobales genomes encode one α subunit and two β subunits that make up the 20S core particle. The α subunits assemble into homo-heptameric rings whereas the two types of β subunits form hetero-heptameric rings[32]. In agreement with its role in cell division, proteasome is crucial for the cells since all the subunit genes are likely essential in *Sa. islandicus*[33]. Homologs of proteasome assembly factors are present in archaea, some of which have been characterized[34,35]. However, it remains elusive how the proteasome is *do novo* assembled in archaeal cells and if this process is associated with phosphorylation-mediated regulation.

Archaeal protein kinases and phosphatase are more similar to their eukaryotic counterparts than to those found in bacteria[36]. Eukaryotic protein kinases (ePKs) can be classified into typical and atypical categories, with the former harboring 12 conserved classical subdomains whereas the later lacking sequence similarity[37,38]. The genomes of Sulfolobales encode 9–11 ePKs[36]. Studies have shown that archaeal atypical ePKs, such as Bud32, Rio1 and Rio2 homologs, perform conserved roles in tRNA modification and ribosome biogenesis, respectively, similar to their counterparts in eukaryotes[39,40]. In addition, it was reported that typical ePKs in Sulfolobales are involved in a complex regulation network that governs various

cellular processes including cell mobility, biofilm formation, DNA damage response, and DNA repair[41-45]. However, it remains unclear whether archaeal ePKs play a role in cell cycle regulation.

In this study, we reveal that ePK2 in *Sa. islandicus* exhibits a cyclical expression pattern with a peak during cell division at the protein level. Additionally, the α subunit of the proteasome (PsmA) was identified as a substrate of ePK2. Phosphorylation of PsmA affects proteasome assembly and regulates its activity, thereby controlling cell division progression. This study has identified an innovative and effective mechanism for regulating cell division in Sulfolobales archaea. This mechanism involves ePK-mediated proteasome phosphorylation and serves as a prototype for understanding the regulation of the eukaryotic cell cycle.

Results

The ePK2 gene is expressed cyclically in *Sa. islandicus*

In eukaryotes, protein phosphorylation plays a crucial role in cell cycle control[3]. Previous studies have shown that two ePKs, Saci_1193 and Saci_1694, in *S. acidocaldarius* were transcribed in a cell cycle-dependent manner[46]. Saci_1193 was significantly induced alongside genes related to chromosome segregation and cell division[46]. The genome of *Sa. islandicus* REY15A encodes a homolog of Saci_1193 (SiRe_2030). Transcriptomic analysis indicates that the transcription of *sire_2030* changes in a cell cycle dependent manner alongside with genes involved in chromosome segregation and cell division, while the transcription of other protein kinases does not exhibit a clear cyclical pattern[29] (Fig. 1A and Fig. S1). To validate the cyclical pattern of ePK2, cells were synchronized at the G2 phase by treating with acetic acid for 6 h. After the acetic acid was washed out, the cells were cultured in fresh medium and allowed to progress through the cell cycle (Fig. 1B and 1C). Cell samples were collected at specified time points for RT-qPCR (Fig. 1D). The result revealed that *ePK2* mRNA gradually increases after release, peaking at about 2 h,

consistent with the transcriptomic data. To assess whether the expression changes cyclically at protein level, Western blotting analysis was conducted and the results revealed that the SiRe_2030 level follows a cyclical pattern, peaking around 3 h after release (Fig. 1E). These results suggest that SiRe_2030, named as SisePK2 hereafter, and its homologs in Sulfolobales likely play a role in regulating cell cycle progression.

Deletion of e*PK2* leads to impaired cell cycle progression

To investigate the role of ePK2 in cell cycle regulation, we constructed a deletion strain Δ*ePK2* (Fig. S2A and S2B) and characterized its phenotype by measuring cell growth and microscopy. Interestingly, we found that while asynchronized cells of Δ*ePK2* did not show apparent growth retardation and abnormality in cell morphology and cell cycle progression (Fig. 2A-2D), synchronized cells displayed distinct flow cytometry profiles compared with the wild type E233S (Fig. 2E). In the wild type cells, the number of G1 cells gradually increased at 2 h after release from G2 and peaked at 4 h. However, in Δ*ePK2* cells, the G1 peak was barely detected within 6 h after release, suggesting a deficiency in cell cycle progression caused by a failure in chromosome segregation or cell division, or a decoupling of cell division and the initiation of DNA replication To further investigate whether the absence of the G1 peak depends on the ePK2 kinase activity, we constructed two strains with in-frame catalytic deficient mutations, ePK2-D498A and ePK2-D532A (Fig. S2C and S2D). The flow cytometry profiles of the two synchronized strains resembled those of Δ*ePK2*, suggesting that the deficiency in cell cycle progression was due to the absence of ePK2 kinase activity (Fig. 2E). These results indicate that ePK2 and its kinase activity play an essential role in facilitating cell progression from G2 to G1 and suggest that phosphorylation of ePK2 target(s) may be involved in regulating chromosome segregation or cell division.

Overexpression of ePK2 impairs cell division

To further explore the *in vivo* function of ePK2, we constructed an ePK2 overexpression strain based on the shuttle vector pSeSD with an arabinose-inducible promoter[47]. We found that overexpression of ePK2 led to the formation of enlarged cells (2.460 ± 0.528 μm vs 1.209 ± 0.173 μm) and inhibited cell growth (Fig. 3A-3C). Flow cytometry analysis showed that cells with multiple copies of chromosomes (>2C) were produced, indicating that although cell division was impaired, genome replication remain unaffected (Fig. 3D). To determine whether the inhibition was dependent on the kinase activity of ePK2, we constructed a strain overexpressing a point mutant of ePK2 on the conserved catalytic residues K393 and D498 (ePK2-K393A/D498A). Our results showed that the ePK2-K393A/D498A overexpression strain exhibited only slightly slower growth compared to the control harboring the empty vector but performed much better than the ePK2 overexpression strain (Fig. 3A). Moreover, the average cell size only slightly increased as compared to that of the wild type (1.680 ± 0.370 μm vs 1.209 ± 0.173 μm) (Fig. 3B and 3C). These results suggest that the growth inhibition observed in the ePK2 overexpression strain was largely dependent on its kinase activity. Furthermore, our study revealed that the G1 peak of synchronized ePK2 overexpression strain was absent, and the DNA content gradually increased after cells were released from G2 phase (Fig. 3E). This indicates that overproduced ePK2 significantly hinders chromosome segregation or cell division, but not genome replication. These results also imply that phosphorylation of ePK2 target(s) needs to be strictly regulated for normal cell cycle progression, such as accurate chromosome segregation/cell division or DNA replication initiation.

The α subunit (PsmA) of *Sa. islandicus* proteasome is a substrate of ePK2

To identify potential substrates or interactors of ePK2, His-tagged ePK2 was expressed in *Sa. islandicus* using the overexpression strain and purified by Ni-NTA and gel filtration. SDS-PAGE analysis of the samples identified four co-purified bands in fraction 11, preceding the ePK2 peak (fraction 12) (Fig. 4A). Mass

spectrometry (MS) analysis revealed that the co-purified proteins included thermosomes (SiRe_1214 and/or SiRe_1716), fructose-1,6-biphosphate aldolase/phosphatase (Fbp), and proteasome α subunit (PsmA). To determine whether ePK2 directly phosphorylates PsmA, an *in vitro* kinase assay was performed using purified proteins from *E. coli*. Phosphorylated proteins were detected by Western blotting with an antibody specific for phosphorylated Thr/Tyr. As shown in Fig. 4B, the wild type ePK2, but not the kinase-dead mutant ePK2-K393A/D498A/D532A, was able to phosphorylate PsmA. Additionally, the intensities of phosphorylation signals increased with increasing concentrations of PsmA. Furthermore, the specificity of PsmA phosphorylation by ePK2 was confirmed by comparing its phosphorylation by another protein kinase ePK1 (SiRe_2056), known for its higher activity with a broad substrate range *in vitro*[45]. As illustrated in Fig. 4C, the phosphorylation signal of PsmA by ePK1 was much weaker than that observed with ePK2, indicating that PsmA was specifically phosphorylated by ePK2 but not ePK1.

Overexpression of ePKs resulted in accumulation of cell division proteins

Previous studies have shown that cyclically expressed cell division protein CdvB is a target of the proteasome, and failure to degrade CdvB by proteasome impairs cell division in both *S. acidocaldarius* and *Sa. islandicus*[19,28]. This suggests that proteasome activity is crucial for cell division in Sulfolobales. Since PsmA is a substrate of ePKs, we hypothesized that overexpression of ePK2 might affect the proteasome activity, leading to deficiency in cell division. To test this, we compared the CdvB levels in synchronized cells of wild type and ePK2 overexpression strains using Western blotting. In wild type cells, CdvB accumulated at 1–2 h after release from G2 and was rapidly degraded after 3 h, coinciding with completion of cell division in most cells (Fig. 5A). In contrast, in cells of the overexpression strain, the degradation of CdvB was apparently delayed until 5 h after release from G2, indicating that the proteasome activity was impaired in this strain (Fig. 5A). In addition, we also examined the levels of other cell division protein, CdvB1 and

CdvB2, which work in conjugation with CdvB[18,19,28]. Treatment with Bortezomib, a proteasome-specific inhibitor, resulted in accumulation of CdvB1 and CdvB2, indicating they are also targets of the proteasome (Fig. S3A). Notably, we found that although CdvB1 displayed cyclical expression pattern, its degradation was delayed and slower compared to that of CdvB (Fig. 5A), consistent with its role at late stage in cell division[18,19,28]. As expected, degradation of CdvB1 was also inhibited upon ePK2 overexpression (Fig. 5A). Next, we detected the levels of CdvB1 and CdvB2 in asynchronized culture of ePK2 overexpression strain. As depicted in Fig. 5B, the overexpression strain exhibited approximately 8 times higher levels of ePK2 compared to the wildtype strain and the levels of both CdvB1 and CdvB2 were significantly increased with ePK2 overexpression. To rule out the possibility that the accumulation of cell division proteins in the cell was a result of increased *cdvB1/cdvB2* transcription, we assessed both mRNA and protein levels at different time points following ePK2 induction. We observed that CdvB1 protein increased by approximately 2-fold after 6 h of induction, while its mRNA level only slightly increased after 8 h of induction and even decreased before 8 h (Fig. S4). These finding suggest that the elevation in CdvB1 protein level was attributed to its reduced degradation by the proteasome rather than increased transcription. In addition, the protein levels of two proteasome subunits, PsmA (SiRe_1271) and PsmB1 (SiRe_1237), were comparable to those of the wild type (Fig. 5B), suggesting that the proteasome content in the ePK2 overexpression strain remained unchanged.

ePK2 phosphorylation inhibits cellular proteasome activity

To determine whether the proteasome activity was impaired in the ePK2 overexpression strain, we measured the proteasome activity of whole cell lysate using a fluorescent substrate, Suc-LLVY-AMC [48]. Our finding revealed that the proteasome activity of the total soluble cell extract was significantly reduced in the ePK2 overexpression cells as compared with that in cells harboring empty vector pSeSD (Fig. 5C). However, the proteasome activity of ePK2-K393A/D498A overexpression

strain was only slightly weaker than the control, consistent with our previous result that the inhibition was mainly dependent on the kinase activity of ePK2 (Fig. 5C). Furthermore, Western blotting showed that both CdvB1 and CdvB2 accumulated in ePK2 overexpression strain, while the ePK2 mutant overexpression only led to partial accumulation of these proteins (Fig. 5D). As expected, in Δ*ePK2* neither the proteasome activity nor accumulation of CdvB1 and CdvB2 was significantly different from those in strain E233S, in agreement with the result that the phenotype of ΔePK2 cells was similar to that of E233S under asynchronization conditions (Fig. 5C and 5D). This observation raises the possibility that there might be other protein kinase(s) playing redundant role in the asynchronized cells. Taken together, we conclude that overexpression of ePK2 inhibits cellular proteasome activity in *Sa. islandicus*.

ePK2 deletion results in accelerated degradation of cell division proteins, causing impaired cytokinesis and ultimately cell death

To further investigate the impact of the absence of ePK2 on cell division, we examined levels of cell division proteins in synchronized Δ*ePK2* cells releasing from G2 phase using Western blotting. Strikingly, levels of CdvB and CdvB1 were significantly reduced in synchronized Δ*ePK2* cells compared to the wild type E233S (Fig. 5E). Moreover, cells with catalytic deficient mutations, ePK2-D498A and ePK2-D532A, also exhibited lower levels of CdvB1 than E233S after synchronization (Fig. S3B). These results indicate that, opposite to ePK2 overexpression, cells without ePK2 may lead to abnormally high proteasome activity resulting in failure in accumulation of CdvB proteins post-G2 phase and subsequent impaired cell division (Fig. 2E). Analysis of synchronized cells incubated for more than one cell cycle (typically 6 h) using flow cytometry revealed that increasing numbers of Δ*ePK2* cells contained <1C genomic DNA after 10 h release (Fig. 5F). This indicates that these cells failed to undergo cell division and gradually died in the absence of ePK2.

ePK2 phosphorylates PsmA at S200 and T213

To identify the phosphorylated residues of PsmA by ePK2, we performed comparative quantitative phosphoproteomic analysis between ePK2 overexpression strain and the control. The result showed that phosphorylation of 434 sites (from 305 proteins) increased by over 2-fold in ePK2 overexpression strain, among which 43 residues (from 38 proteins) increased by over 10-fold (Table S4). Thermosomes, Fbp, and PsmA are proteins with phosphorylation sites increased over 10-fold. Four residues (S46, S59, S200, and T213) on PsmA were phosphorylated and the phosphorylation at S200 and T213 increased by 2.7-fold and 11.7-fold, respectively, with ePK2 overexpression (Fig. 6A, Table 1). To verify these residues were phosphorylated, wild type PsmA and its single, double or multiple point mutants were purified from *E. coli* and subjected to a kinase assay with ePK2. Radiolabeled [γ-^{32}P] ATP was used to quantify the phosphorylation levels. As shown in Fig. 6B and 6C, although phosphorylation of S200A (102.0%) did not decrease compared to the wild type PsmA, phosphorylation of T213A was reduced to 75.7% and that of the double mutant S200A/T213A decreased further to 38.8%, suggesting that ePK2 phosphorylated both S200 and T213 of PsmA. However, phosphorylation of S46A/S59A/S64A/T213A (78.1%) and S46A/S59A/S64A/S200A/T213A (51.0%) did not decrease further, compared to those of T213A and S200A/T213A, respectively, indicating that S46A/S59A/S64A is not the targets of ePK2 *in vitro*. Alternatively, there could be interplay between phosphorylated sites. Taken together, we revealed that ePK2 phosphorylates PsmA at both S200 and T213 *in vivo* and *in vitro*.

Overexpression of PsmA phospho-mimic mutants S200D and T213E has pronounced and modest impacts on cell division, respectively

To explore the functional mechanism of PsmA phosphorylation, we initially attempted to delete *psmA* in *Sa. islandicus* E233S. Consistent with previous findings from a genome-wide transposon mutagenetic analysis[33], we were unable to obtain a *psmA* knockout strain, confirming its essential role in cell viability. Next, we constructed strains overexpressing the wild type PsmA and its phosphorylation site mutants

including dephosphorylation mutants S200A, T213A, and S200A/T213A, as well as phospho-mimic mutants S200D, T213E, and S200D/T213E. Increased levels of PsmA proteins (approximately 3–5 folds) were observed in the overexpression strains compared to cells harboring the empty vector (Fig. S5). As depicted in Fig. 7A and 7B, overexpression of wild type PsmA resulted in growth retardation and cell enlargement (1.560 ± 0.287 μm vs 1.274 ± 0.155 μm), although to a lesser extent compared to the ePK2 overexpression strain. In addition, PsmA overexpression did not affect genome replication since the enlarged cells were found to contain more than 2 copies of chromosomes as revealed by flow cytometry (Fig. 7C). These results indicate that PsmA overexpression impaired the proteasome activity and inhibited cell division, reminiscent of the ePK2 overexpression strain's phenotypes. To validate this, we examined the CdvB1 level and proteasome activity in the PsmA overexpression cells. As anticipated, the CdvB1 level increased and the proteasome activity was inhibited (Fig. 7D and 7E). Furthermore, CdvB1 degradation was significantly slower in the PsmA overexpression strain compared to the wild type, as revealed by Western blotting of synchronized cells (Fig. S6), suggesting a deficiency in proteasome-mediated degradation. We assume that PsmA overexpression may affect correct proteasome assembly and impair its activity *in vivo* (see below).

Surprisingly, all dephosphorylated mutant overexpression cells (S200A, T213A, and S200A/T213A) exhibited a similar phenotype to that of wild type overexpression cells (Fig. 7). Intriguingly, overexpression of phospho-mimic mutants, S200D and T213E, had contrasting effects on the cells: S200D overexpression further inhibited cell growth and cellular proteasome activity, while T213E overexpression basically did not influence the growth and CdvB1 degradation, and its proteasome activity was only slightly reduced as compared with that of Sis/pSeSD (Fig. 7 and Fig. S6). Moreover, overexpression of the double phospho-mimic mutant S200D/T213E had the same effect as T213E (Fig. 7 and Fig. S6), indicating that phospho-mimic mutation of T213 somehow neutralized the severe effect of S200D on the cell. We speculate that mutation of S200 and T213 to alanine did not affect their inter-subunit

interaction and interactions with other factors, resulting in a similar phenotype to WT overexpression. On the other hand, mutation of S200 and T213 to negative-charged phospho-mimic residues abolished all or part of these interactions. In addition, the effect of T213E may be upstream of that of S200D.

Phosphorylation of residues S200 and T213 does not affect the interaction between α subunits

In order to elucidate the different effects of S200D and T213E overexpression on cells and uncover potential regulatory mechanism through PsmA phosphorylation, we isolated proteasomes in cells overexpressing His-tagged wild type PsmA and its mutants, and characterized them by SDS-PAGE, Western blotting, and microscopy with a Focused Ion Beam Scanning Electron Microscope. Notably, we were able to observe the co-purified non-tagged PsmA band encoded by the genome and the quantity of non-tagged PsmA co-purified with His-tagged T213E was apparent lower than that of the His-tagged PsmA (Fig. S7A). However, the migration of His-tagged S200D and non-tagged PsmA were too close to be differentiated. In addition, one of the two β subunits, PsmB1, were also detected in all three samples (Fig. S7B). Electron microscopy analysis revealed that the majority of proteasome particles consisted of two heptameric rings, instead of 20S core particle with four rings, despite the presence of the β subunit in these samples (Fig. S7C-7E). This was further confirmed by analyzing PsmA purified from *E. coli*, yielding the same result (Fig. S7F). This suggests that the two mutations, or phosphorylation at these two residues, do not affect the interaction between α subunits.

Phosphorylation of S200 disrupts 26S proteasome assembly from 20S whereas phosphorylation of T213 affects *de novo* assembly of α ring in the proteasome

To gain deeper insights into the functional mechanism of S200 and T213 phosphorylation, we conducted an investigation into the assembly of 20S and 26S (20S with proteasome-activating nucleotidase (PAN)) through sucrose density

gradient centrifugation followed by proteasome activity analysis. The result of the Western blotting analysis revealed two signal peaks of PsmB1 in the strain carrying the empty vector, observed at fraction 2 and fractions 8–9, respectively (Fig. 8A). The proteasome activity assay showed that the fractions corresponding to these two signal peaks exhibited the highest peptidase activities, indicating that the fractions 2 and 8–9 contained 20S and 26S proteasomes, respectively (Fig. 8B). To confirm that the observed activity was not attributed to other peptidases in the cell, various protease inhibitors, including PSMF, protease inhibitor mixture, and a proteasome-specific inhibitor Bortezomib, were added in the assay. It was found that Bortezomib but not any other protease inhibitor suppressed the activity (Fig. 8B). Furthermore, addition of ePK2 in the reaction mixtures led to a partial inhibition of the protease activities in both fractions, confirming that phosphorylation of 20S proteasome subunit impair its functionality (Fig. 8B).

We observed that the two signal peaks of wild type PsmA overexpression cells shifted from factions 2 and 8–9 to fractions 2–4 and 8–10, respectively (Fig. 8A). Proteasome activity also showed similar shifts. Nevertheless, the specific fractions containing 20S/26S proteasomes in wild type PsmA overexpression cells exhibited lower peptidase activities compared to cells carrying the empty plasmid (Fig. 8C). This suggests that overproduction of PsmA disrupts the assembly of normal 20S and 26S proteasomes by potentially overloading the α subunit, resulting in the formation of 20S/26S proteasomes with higher molecular weights but decreased activities. This may explain the observed phenotype in the wild type PsmA overexpression strain. Strikingly, in S200D overexpression strain, only the 20S proteasome peak was present while the 26S proteasome peak was completely absent (Fig. 8A). The proteasome activity assay also showed a lack of peptidase activity at the position where the 26S proteasome typically appears (Fig. 8C), suggesting a failure of the 26S proteasome assembly in the cell.

It has been demonstrated that the activation of 20S proteasome is triggered by the

interaction of an HbYX motif at the C-terminus of PAN with the conserved Lys of PsmA, leading to the opening of 20S gate[49-51]. As a control, a strain overexpressing PsmA with a mutation at the conserved Lys, K68A, was constructed. As expected, we observed a significant decrease in both the 26S proteasome signal and activity peaks in K68A overexpression strain, similar to what was observed in the S200D overexpression strain (Fig. S8A and S8B). Furthermore, we found that the sediments and activities of the 20S and 26S proteasomes in the T213E overexpression strain were comparable to those observed in the Sis/pSeSD strain (Fig. 8A and 8C), aligning with their corresponding phenotypes (Fig. 8). The results imply that overproduced T213E in the cell could not be incorporated into the 20S/26S proteasomes. This was consistent with our previous finding that purified T213E from its overexpression strain only pulled down lesser amounts of genome-encoded PsmA (Fig. S7A), suggesting that T213E formed α rings on its own but faced challenges in being integrated into functional internal α rings assembled *de novo*. Expectedly, the analysis of S200D/T213E overexpression strain using sucrose density gradient centrifugation revealed a pattern identical to that of T213E and the control strain with an empty vector, indicating that failure of S200D/T213E to be incorporated into functional internal α rings due to the T213E mutation would erase the effect of S200D mutation (Fig. S8A and S8B). In summary, our findings suggest that phosphorylation of S200 abrogates 20S-PAN assembly, whereas phosphorylation of T213 may affect *de novo* α ring assembly.

Structural modelling of the wild type and mutant PsmA proteins and the α rings

To investigate the potential molecular mechanisms behind the impact of S200 and T213 phosphorylation on the assembly of 20S/26S proteasome in *Sa. islandicus*, the structures of PsmA carrying these mutations and the assembled α rings were generated using Alphafold3. The monomeric structure T213E mutant closely resembled that of the wild type PsmA, with a slight misalignment at its N-terminus being the only difference (Fig. 8D). However, S200D exhibited a notable elongation

of the α helix at the N-terminus with a further dislocation. In the predicted whole α rings, the wild type PsmA and T213E assembly are almost the same with the N-termini of seven monomers being arranged as a lid-like structure above the central channel of proteasome (Fig. 8E). On the other hand, the N-terminal α helix of S200D shifts deeper into the central channel, causing a disruption in the proper alignment of the N-termini from each monomer above the channel. This resulted in a structure with only four N-termini being visible while three are predicted to be buried down into the channel as loops (Fig. 8E). The structural change in the N-terminus of S200D may impede the interaction between PsmA and PAN, leading to a failure in the assembly of 26S proteasome. So far, the reason for the inability of T213E to be incorporated into α ring remain unclear, since there is minimal disparity observed in the structural models. This may suggest that there is a complex *de novo* assembly process of the α ring or the 20S proteasome which requires additional assembly factors *in vivo*. Supporting this notion, we have identified two potential 20S proteasome assembly factors (SiRe_1724 and SiRe_1163) that co-purified with PsmA in mass spectrometry analysis of *in vivo* protein samples (data not shown). The mechanisms behind the assembly of the 20S/26S proteasome in *Sa. islandicus* warrant further investigation in future studies.

Discussion

The order Sulfolobales of Archaea exhibit distinct cell cycle phases and serve as excellent models for investigation into cell cycle regulation mechanisms in early life forms. Previously, it has been shown that levels of cell division proteins in Sulfolobales are controlled by proteasome-mediated degradation and by the cyclical expression of the transcription factor aCcr1[28,29]. Here, we demonstrate that a cyclic ePK-mediated phosphorylation plays a role in regulating proteasome assembly, hence influencing the proteasome's degradation activity towards proteins like CdvBs and dictates cell cycle progression in *Sa. islandicus*. The finding of this study implies that Sulfolobales archaea have a prototype of phosphorylation-mediated cell division

regulation mechanism.

Multiple phosphorylation residues in PsmA including S200 and T213 were identified through phosphoproteomic analysis of ePK2 overexpression cells. However, attempts to identify phosphorylated S200 and T213 of PsmA purified from asynchronized culture using Co-IP with anti-PsmA were unsuccessful, suggesting that this type of phosphorylation may be transient and limited to a specific period during the cell cycle (late M phase). Rapid dephosphorylation by active phosphatases likely follows to ensure precise control and efficiency in cell division[52]. This regulation is essential since the window for cytokinesis during cell division in Sulfolobales archaea is extremely short, e. g. only less than 7 min in *S. acidocaldarius*[53].

In eukaryotes, the assembly of 20S proteasome is a complex process that involves several chaperons, Pba1–4 and Ump1 in yeast (PAC1-4 and POMP in mammals). The Pba1-Pba2 complex is responsible for appropriate incorporation of α subunits into α ring and prevents premature binding of the 19S particle to the α ring[54-56]. Additionally, Pba3-Pba4 and Ump1 are required for incorporation of β subunits and Ump1 prevents inappropriate dimerization of two half-proteasomes[57-59]. Recent Cryo-EM analysis has revealed the order of incorporation of α and β subunits during human 20S proteasome assembly. It was shown that PAC1-PAC4 have extensive contacts with α5, α6 and α7 with the C-termini of PAC1 and PAC2 inserting into the HbYX binding pockets between α subunits[60]. Our results suggest that phosphorylated T213 may be not incorporated into α ring during its *de novo* assembly. Indeed, a very limited amount of genome-encoded PsmA was pulled down when T213E was purified *in vivo* compared to WT (Fig. S7A). Although assembly of an archaeal 20S particle can be accomplished by co-expression of α and β subunits in *E. coli* without additional partners, the characterization of Pba homologs suggested that they may play a role in the assembling process in archaea[34,35]. Interestingly, two putative Pba1/2 homologs, SiRe_1163 and SiRe_1724, were identified in our MS analysis of the pull-down samples using PsmA antibody (data not shown), suggesting that 20S proteasome

assembly may also need chaperons in archaeal cells. Since Pba/PAC complexes interact with multiple α subunits through HbYX binding pockets in both archaea and eukaryotes and T213 locates at a loop adjacent to the HbYX binding pocket (Fig. 8D), mutation of T213E may disrupt the interaction of PsmA with the putative Pba complex and prevent the incorporation of T213E into the *de novo* α ring. Several lines of evidences from this study together strongly suggest that phosphorylation at S200 blocks the interaction between the 20S particle and PAN, resulting in a failure in 26S assembly (Fig. 7, Fig. 8 and Fig. S8), while phosphorylation of T213 may block α ring assembly. Further investigation is required to fully understand the role of these residues in 20S/26S assembly.

In eukaryotes, proteasome activities are regulated by phosphorylation of various subunits. For example, T25 of the 19S subunit Rpt3, a conserved residue among vertebrate, is phosphorylated during the G2/M phase to facilitate efficient protein translocation for degradation and cell proliferation, while phosphorylation of S361 of Rpn1 and S16 of α5 impair 26S proteasome assembly and cell proliferation[7,8,61]. Recently, in response to DNA damage, phosphorylation of Rpn10-S266 alters the conformation of its two ubiquitin-interacting motif, resulting in reduced binding to ubiquitinated DNA repair proteins and subsequent degradation for efficient DNA repair[9]. Our study demonstrates that, phosphorylation of α subunit, PsmA-S200 in *Sa. islandicus* impairs 26S proteasome assembly, akin to the effect of Rpn1-S361 phosphorylation in eukaryotes[7]. We speculate that PsmA-T213 phosphorylation may disrupt its interaction with Pba1/2 homologs and impair its incorporation into the *de novo* α ring, an early step of 20S proteasome assembly. Similarly, the eukaryotic α5-S16 residue is buried at the 19S-20S interface and its phosphorylation only occur in the free form of α5 or in protein complexes too small to be proteasomes[8], indicating that this phosphorylation also impair the early assembly of the 20S proteasome. Moreover, our current and previous phosphoproteomic analysis[43] have identified phosphorylation of S46, S59 and S64 in PsmA, in addition to S200 and T213. The proximity of S59 and S65 to the conserved K68A suggests that they may directly

impact the activation of the 20S proteasome by PAN. Therefore, it is likely that phosphorylation of different residues in PsmA confer various strategies for proteasome regulation, similar to those in eukaryotes.

Although phosphorylation occurs at multiple residues of archaeal PsmA, none of them are conserved in Sulfolobales as revealed by sequence alignment (Fig. S9). In contrast, phosphorylated residues in several subunits of eukaryotic proteasomes are highly conserved[7,8,61], suggesting that phosphorylation-mediated regulation of proteasomes in eukaryotes may already exist in FECA, the first eukaryotic common ancestor. However, phosphorylation on archaeal PsmA might vary among different species while still serving similar functions, implying an early form of proteasome regulation by post-translational modification.

We observed that Δ*ePK2* did not display any apparent differences with the wild type in terms of cell growth, morphology, and flow cytometry profile when not synchronized (Fig. 2A-D). However, synchronized Δ*ePK2* cells exhibited a deficiency in cell cycle progression deficiency with a lack of G1 peak and failure in cell division, presumably resulted from elevated degradation of CdvBs (Fig. 2E, 5E and 5F). It is possible that in asynchronized cells, PsmA would be phosphorylated by other protein kinase(s) that are constantly expressed throughout the entire cell cycle, albeit less efficiently (Fig. S1). In agreement with this, our *in vitro* kinase assay showed that ePK1, another highly active kinase, was also able to phosphorylate PsmA, although to a lesser extent than ePK2 (Fig. 5C). Furthermore, ePK2 contains multiple tetratricopeptide repeats (TPR) that could potentially recruit other protein kinases (or partners) through protein-protein interaction for phosphorylation of S46, S59 and S65 *in vivo* which are not directly targeted by ePK2[62]. We speculate that treatment of Sulfolobales cells with acetic acid would induce a quiescent stage during which protein activities are reduced. In such conditions, the complementary phosphorylation by other kinases may not function efficiently, leading to the assembly of active proteasome and a failure in reducing cellular proteasome activity. It would be

interesting to investigate which kinase phosphorylates these residues and how the phosphorylation works. However, the lack of G1 peak in synchronized Δ*ePK2* cells and uncontrolled DNA replication in the enlarged cells overexpressing ePK2 may also indicate a decoupling of cell division and the initiation of DNA replication. Therefore,, exploring other targets of ePK2 and the proteasome or utilizing alternative synchronization methods, such as the baby machine method[63] or treating with the translation inhibitor tetracycline[64,65], could help elucidate the phenotypic discrepancy between synchronized and asynchronized cells.

To summarize, our study demonstrates that protein phosphorylation plays a vital role in regulating the cell cycle progression of archaea. Based on our findings, we propose a model depicting ePK2 phosphorylation on the proteasome α subunit for cell division regulation in Sulfolobales (Fig 9). Following the G2 phase, the expression of ePK2 gradually increases in conjunction with cell division proteins. This leads to the inhibition of proteasome activity through the phosphorylation of the α subunit at S200 and T213 by ePK2. This dual phosphorylation events prevent the assembly of the 26S proteasome (S200 phosphorylation) and results in the formation of active 26S proteasome (T213 phosphorylation), ultimately leading to the stabilization of cell division proteins CdvB/CdvB1/CdvB2 at mid-cell. During the subsequent D phase, the down-regulation of ePK2 allows for the assembly and activation of proteasomes for degradation of CdvB proteins. Furthermore, reduced transcription of CdvB genes by aCcr1 will also facilitate preventing the accumulation of CdvBs. The coordinated action results in the progression of cell division through ring constriction and membrane abscission. When ePK2 is overproduced during M phase, continuous inhibition of the proteasome leads to the accumulation of CdvB proteins, causing cells to enlarge and exhibit increased DNA contents due to decoupling between cell division and DNA replication. Future work will focus on how phosphorylation affects proteasome assembly and how the eukaryotic proteasome phosphorylation mechanisms evolved from archaea especially Asgard archaea.

Materials and methods

Strains and growth conditions

The *pyrEF* and *lacS* deficient mutant *Sa. islandicus* REY15A (E233S) (hereafter E233S) and its derivatives were grown at 75 °C in STVU medium (basal salts supplemented with 0.2 % (w/v) sucrose (S), 0.2 % (w/v) tryptone (T), a mixed vitamin solution (V), and 0.01 % (w/v) uracil). The pH was adjusted to 3.3 with sulfuric acid as described previously[44]. E233S carrying the shuttle vector pSeSD with or without genes were grown in STV medium. The ATV was used for protein overexpression in *Sa. islandicus*, where sucrose was replaced with 0.2 % (w/v) D-arabinose (A). The solid medium was prepared using gelrite (0.8 % [w/v], Sigma, USA). Normally, cells were cultured to OD_{600}=0.6–0.8, then transferred to fresh medium with an initial estimated OD_{600} of 0.05 for growth curve determination. PMSF was purchased from Sangon Biotech Co., Ltd. (Shanghai, China), protease inhibitor mixture and Suc-LLVY-AMC were purchased from MeilunBio (Dalian, China), and bortezomib was purchased from Solarbio (Beijing, China).

Construction of deletion and overexpression strains

Construction of the knockout and site-directed mutant strains was performed according to the endogenous CRISPR-Cas-based genome editing method as described previously[66]. The 40 nt DNA sequence downstream of CCA or TCA motif was selected as the protospacer and annealing of the two complementary oligonucleotides yielded a DNA fragment containing the designed spacer. The spacer fragment was inserted into the digested vector yielding the artificial mini-CRISPR plasmid. The donor DNA fragment was generated by splicing and overlapping extension (SOE)-PCR with *ApexHF* HS DNA Polymerase FS (Accurate Biotechnology, Hunan, China). Then the donor DNA fragment was digested with *Sph*I and *Xho*I and inserted into mini-CRISPR plasmid to generate the genome editing plasmids. The cells of *Sa. islandicus* E233S were transformed with the plasmid by electroporation[67]. The

in-frame deletion and site-directed mutant strains were screened and verified by PCR amplification using the primers check-F and check-R primers and subsequent sequencing of the PCR products. The gene editing plasmid was removed by counter selection with uracil and 5-fluoroorotic acid (5-FOA). The strains, plasmids and the primers used in this study are listed in Supplementary Table S1, Table S2 and Table S3, respectively.

To construct gene overexpression strains, the gene fragments of ePK2 or PsmA were amplified using the genomic DNA of *Sa. islandicus* E233S by PCR and the fragment containing mutant derivative was obtained by SOE-PCR. The resulting DNA fragments were digested and ligated into the vectors pET22b and pSeSD[47] at *Nde*I/*Sal*I site, yielding the expression plasmids for WT and mutant proteins. The sequences of the plasmids were verified by DNA sequencing. The pET22b plasmids were transformed into *E. coli* BL21(DE3) cells for the expression of recombinant proteins. The pSeSD plasmids were introduced into the cells of *Sa. islandicus* E233S by electroporation, yielding *Sa. islandicus* strains for protein overexpression.

Cell synchronization

Cell synchronization was performed as described previously[29]. Briefly, *Sa. islandicus* cells were grown to log-phase and transferred for 3–4 times for activation of the cells. Cell synchronization was conducted by adding 6 mM acetic acid into a culture with OD_{600}~0.2 for 6 h. Then the cells were washed with 20 mM sucrose for 3 times and re-incubated in preheated medium which was set as the start point (0 h). The cells were then released from G2 phase during which samples were taken for flow cytometry and Western blot at 1 h interval or as specified time points.

Microscopy and flow cytometry

Cell morphology were analyzed by microscopy under a NIKON TI-E inverted fluorescence microscope (Nikon, Kobe, Japan). Samples from three independent cultures were examined. For flow cytometry, the culture (0.3 mL) of *Sa. islandicus*

were harvested and fixed with 70 % ice-cold ethanol (final concentration) and stored at 4 °C. After 12 h, the fixed cells were collected by centrifugation at 800 *g* for 20 min and washed twice with 1 mL of PBS buffer. The pellets were resuspended in 150 μL PBS buffer and stained with SUPER Green I (Fanbo Biochemicals, Beijing, China). The stained samples were analyzed by flow cytometry using the ImageStreamX MarkII Quantitative imaging system (Merck, Darmstadt, Germany) equipped with a 488 nm laser. A dataset of at least 20,000 cells was obtained for each sample. For synchronized cell samples, propidium iodide (Sigma-Aldrich) was used for DNA staining.

Quantitative reverse transcription PCR (RT-qPCR)

Cells were collected by centrifugation at 6,000 *g* for 5 min and 1 mL of the SparkZol Reagent (SparkJade, Shandong, China) was added. Total RNA was extracted according to the manufacturer's instructions. The first-strand cDNA was synthesized by reverse transcription of RNA using Evo M-MLV RT Mix Kit (Accurate Biotechnology, Hunan, China) according to the manufacturer's protocol. The mRNA levels were evaluated by RT-qRCR using the SYBR Green Premix *Pro Taq* HS qPCR Kit (Accurate Biotechnology, Hunan, China) on the CFX96 Touch™ Real-Time PCR System (Bio-Rad, Hercules, CA, USA). The two-step PCR amplification standard procedure was as follows: 95 ℃ for 30 s, followed by 40 cycles of PCR that consisted of 95 ℃ for 5 s and 60 ℃ for 30 s. The relative transcription level of the target gene was calculated using the comparative threshold cycle (CT) method ($2^{-\Delta\Delta CT}$)[68], and the TBP or 16S rRNA gene was used as reference. The qPCR primers used in this study are listed in Supplementary Tables S3.

Western blot analysis

An aliquot of cell pellets was resuspended in a 100 μL of Buffer A (50 mM Tris-HCl pH 8.0, 200 mM NaCl, and 5% glycerol) and mixed with 5×SDS-PAGE loading buffer for SDS-PAGE analysis. The proteins in the PAGE gel were transferred onto a

PVDF membrane at 200 mA for 2 h at 4 ℃. The membrane was washed and incubated with a primary antibody (Mabnus, Wuhan, China) and then the secondary anti-rabbit HRP-conjugate antibody (Kermey, Zhengzhou, China) following the standard protocol for Western blot. The band was visualized with Immobilon™ Western Chemiluminescent HRP Substrate (Kermey, Zhengzhou, China) and the image was obtained by Imagequant™ 400 (GE Healthcare, UK). The ePK2, PsmA and PsmB1 specific antibodies were prepared in rabbits using full length proteins expressed in and purified from *E. coli*. Phosphorylated protein was detected with Phospho-Threonine/Tyrosine antibody (#9381S, Cell signaling technology, MA, USA).

Protein purification

The pET22b plasmids carrying ePK2 or PsmA genes were transformed into *E. coli* BL21 (DE3)-CodonPlus-RIL for protein expression. The procedure for protein induction and purification in *E. coli* cells was the same as previously described[45]. Briefly, after induction, the cells were harvested and resuspended in buffer A for lysis by sonication. The soluble fractions were heated at 70 ℃ for 30 min and after centrifugation of 10000 *g* for 20 min the supernatants were purified by a Ni-NTA column and Superdex™ 200 10/300 column subsequently (GE Health, UK). The protein concentration was determined by the Bradford method with bovine serum albumin (BSA) as the standard.

For the purification of proteasomes from various PsmA overexpression strains, 3 L of each sample (OD_{600}~0.4) cultivated in STV medium were collected and resuspended in buffer A for lysis by sonication. The soluble fractions were subjected for purification using a Ni-NTA column and Superdex™ 200 10/300 column. The fractions obtained by gel filtration were analyzed by SDS-PAGE, Western blot and focused ion beam electron microscopy.

Phosphoproteomic analysis

Sis/pSeSD and Sis/pSeSD-ePK2 were cultured in ATV medium to OD_{600} = 0.5–0.6. The cells were collected by centrifugation at 6,000 *g* for 10 min and washed with PBS buffer (137 mM NaCl, 2.7 mM KCl, 10 mM Na_2HPO_4, 2 mM KH_2PO_4).

The cell pellets were resuspended in lysis buffer (4% SDS, 100 mM DTT, 150 mM Tris-HCl pH 8.0). The samples were boiled for 3 min and further sonicated for 2 min. Undissolved cellular debris were removed by centrifugation at 16000 rpm for 15 min. The supernatant was collected and quantified with a BCA Protein Assay Kit (Bio-Rad, USA). Digestion of protein was performed according to the FASP procedure described by Wisniewski et al.[69]. Briefly, 1 mg total proteins was mixed with 10 mM DTT and boiled for 5 min. After addition of 50mM iodoacetamide (in 8 M Urea, 150 mM Tris-HCl pH 8.0), the mixture was incubated for 1 min at 600 rpm followed by 30 min at RT in darkness. Six volumes of cold acetone was added and incubated at -20 ℃ overnight for protein precipitation. After centrifugation at 16000 *g* for 15 min, the protein pellet was washed with acetone for twice and dried in a fune hood. The protein suspension was digested in 150 μL trypsin buffer (Promega) (200 μg trypsin in NH_4HCO_3 buffer) overnight at 37 ℃. Then the peptides were acidified with 0.1% trifluoroacetic acid (TFA), desalted with C18 cartridge (Thermo, USA) and vacuum-dried. The dried peptides were dissolved in 0.1% TFA and desalted by Thermo desalting spin column. Finally, the concentrations of peptides were determined with OD_{280} by Nanodrop device (Thermo, USA).

Peptides were labeled with TMT reagents according to the manufacturer's instructions (Thermo Fisher Scientific). Each aliquot (200 μg of peptide equivalent) was reacted with one tube of TMT reagent, respectively. The labeled peptides were mixed equally, desalted by Peptide desalting spin column (Thermo Fisher Scientific) and vacuum-dried. For phosphopeptide enrichment, Fe-NTA Phosphopeptide Enrichment kit (Thermo. A32992) were used for digested peptide mixtures from each sample according to the manufacturer's instructions. The eluted phosphopeptides were vacuum-dried immediately for fractionation by high pH reverse-phase with

STAGETip C18. The total of 6 phosphopeptides fractions were suspended with 0.1% formic acid (FA) for further LC-MS/MS analysis.

LC- MS analysis were performed on an Easy nLC 1200 chromatographic system (Thermo Fisher Scientific). For phosphoproteomic study, the phosphopeptides were loaded to Trap column (100 μm × 20 mm; 5 μm ReproSil-Pur C18 beads, Dr. Maisch GmbH, Ammerbuch, Germany) followed by a self-packed column (75 μm × 150 mm; 3 μm ReproSil-Pur C18 beads, Dr. Maisch GmbH) using buffer A (0.1% formic acid) for gradient separation.at a flow rate of 300 nL/min. Peptide were eluted as following procedure: 0-2 min, 2%-8% linear Buffer B (0.1% formic acid and 85% acetonitrile); 2-45 min, 8%-28% linear Buffer B; 45-50 min, 28%-40% linear Buffer B; 50-52 min, 40%-100% linear Buffer B; 52-60 min, 100% Buffer B. Fractioned peptides were applied to a Q-Extractive HF-X mass spectrometer for 60 min DDA analysis. For MS data acquisition, full MS scans were surveyed from m/z 350 to m/z 1800 at a resolution of 60,000 at m/z 200 with an AGC target values of 3e6 and a maximum injection time 50 ms. Then data-Dependent top 20 MS/MS scans were applied by higher-energy collision dissociation (HCD) with normalized collision energy 32 at a resolution of 45,000 at m/z 200 with an AGC target values of 1e5 and a maximum injection time 50 ms. The isolation window was set to 1.2 m/z.

The phosphoproteome data were imported into Proteome Discoverer 2.4 for data interpretation and protein identification against the *Sa. islandicus* (strain REY15A) database from Uniprot (downloaded on 01/10/2022, and including 2631 protein sequences), which is sourced from the protein database at https://www.uniprot.org/uniprot/. For phosphoproteome MS spectra were searched with 4.5 ppm mass tolerance for precursor ions and 20 ppm mass tolerance for fragment ions, fully Tryptic restriction and maximal two missed cleavage sites. The modifications were variable phosphorylation (+79.96633) on serine (S), threonine (T) and tyrosine (Y). The search results were filtered and exported with <1% false discovery rate (FDR) at site level, peptide-spectrum-matched level, and protein level,

respectively. MaxQuant analysis was filtered only for those phosphorylation sites that were confidently localized (class I, localization probability > 0.75).

For phosphoproteomic data, the t-test (P value) analysis and fold change (FC) was followed and used to determine statistical significance (Q < 0.2) for each comparison. Expression data were grouped together by hierarchical clustering according to the peptide level. To annotate the sequences, information was extracted from Kyoto Encyclopedia of Genes and Genomes (KEGG), and Gene Ontology (GO). GO and KEGG enrichment analyses were carried out with the Fisher's exact test, and FDR correction for multiple testing was also performed.

In vitro kinase activity assay

For the phosphorylation activity assay of the protein kinases on PsmA (or its mutants), indicated amounts of protein kinases and PsmA were added into a reaction mixture (20 μL) containing 25 mM Tris-HCl pH 8.0, 5 mM NaCl, 5 mM $MgCl_2$, 1 mM DTT, and 1 mM ATP). The mixture was incubated at 65 ℃ for 30 min and the reaction was stopped by adding 5×SDS-PAGE loading buffer and boiling for 10 min. The samples were analyzed by 15% SDS-PAGE and Western blot with Phospho-Threonine/Tyrosine antibody. For *in vitro* kinase assay using radiolabeled [γ-^{32}P]ATP, the cold ATP was replaced with 160 nM [γ-^{32}P]ATP (111 TBq/mmol, Hartmann Analytic, Germany). The autoradiographs were quantified by the software ImageQuant 5.2.

Focused ion beam electron microscopy

The protein particles in the PsmA samples purified from *Sa. islandicus* were analyzed by focused ion beam electron microscopy. The protein samples (1-1.5 mg/mL) were dropped onto a carbon film supported copper mesh and stained with 1% acetic acid for 30 s. After dried by an infrared lamp, the samples were observed under a ZEISS crossbeam 550 electron microscope in the STEM model.

Sucrose density gradient fractionation

For detection of proteasome oligomerization and association profiles, a volume of 20 mL *Sa. islandicus* cells (OD_{600}~0.3-0.4) was collected and resuspended in 1 mL of Buffer A. After sonication, the samples were centrifuged at 20,000 *g* for 30 min at 4 ℃. The supernatants (0.5 mL) were layered on top of 12 mL of 5–25% sucrose gradients made in a buffer (containing 50 mM Tris-HCl pH 7.5, 150 mM NaCl, 10% glycerol). Separation of the gradients was performed in a centrifuge with a Beckman SW41 rotor for 20 h at 35000 rpm at 4 ℃. The gradients were fractionated from the top of the sucrose mixture into 500 μL aliquots. Aliquots (20 μL) of the fractions were analyzed by Western blot with PsmB1 antibody. All experiments were repeated at least three times.

Proteasome activity assay

The proteasome activity of whole cell lysis was evaluated by the Fluorescence substrate Suc-Leu-Leu-Val-Try-AMC (Macklin, Shanghai, China). A volume of 20 mL *Sa. islandicus* cells (OD_{600}~0.3–0.4) was collected and resuspended in 1 mL of Buffer A for lysis by sonication. The concentrations of total proteins in the soluble fractions were determined by the Bradford method. An aliquot of 0.5 μg total protein samples was applied for the proteasome activity assay in a 100 μL reaction containing 50 mM Tris-HCl pH 7.5, 250 mM sucrose, 5 mM $MgCl_2$, 1 mM DTT, 2 mM ATP, and 20 μM Suc-LLVY-AMC. The reaction mixture was incubated at 70 ℃ for 30 min. The fluorescence signals were detected by PerkinElmer enspire microplate spectrometer with excitation at 345 nm and emission at 445 nm (CT, USA).

Protein structure prediction

The monomers and α ring structures of wild type PsmA, S200D, and T213E were predicted by Alphafold server (https://alphafoldserver.com/about). The structures were aligned and analyzed using the software PyMOL.

Data availability

All data supporting the findings of this study are available within the article and its Supplementary Information, or from the corresponding author upon reasonable request. The mass spectrometry proteomics data have been deposited to the ProteomeXchange Consortium via the PRIDE partner repository with the dataset identifier PXD061899.

Funding

National Natural Science Foundation of China [32393973 and 32370033 to Y.S.; 31900055 to Q.H.; 31970119 to J.N.]. National Key Research and Development Program of China [2020YFA0906800].

Conflict of interest statement

None declared.

Acknowledgements

We would like to thank the former lab members, Fan Zhou and Dr. Junfeng Liu, for initial work on this project. We are grateful to Prof. Buzz Baum at MRC laboratory for insightful suggestions. Thanks all the lab members of the CRISPR and Archaea Biology Research Centre for helpful discussions and technicians from the Core Facilities for Life and Environmental Sciences, State Key Laboratory of Microbial Technology of Shandong University for assistance.

Reference

1. Pennycook, B.R. & Barr, A.R. Restriction point regulation at the crossroads between quiescence and cell proliferation. *FEBS Lett* (2020).
2. Swaffer, M.P., Jones, A.W., Flynn, H.R., Snijders, A.P. & Nurse, P. CDK Substrate Phosphorylation and Ordering the Cell Cycle. *Cell* **167**, 1750-1761 e16 (2016).

770 3. Matthews, H.K., Bertoli, C. & de Bruin, R.A.M. Cell cycle control in cancer. *Nat Rev*
771 *Mol Cell Biol* **23**, 74-88 (2022).
772 4. Fisher, R.P. The CDK Network: Linking Cycles of Cell Division and Gene Expression.
773 *Genes Cancer* **3**, 731-8 (2012).
774 5. Simmons Kovacs, L.A., Orlando, D.A. & Haase, S.B. Transcription networks and
775 cyclin/CDKs: the yin and yang of cell cycle oscillators. *Cell Cycle* **7**, 2626-9 (2008).
776 6. VerPlank, J.J.S. & Goldberg, A.L. Regulating protein breakdown through proteasome
777 phosphorylation. *Biochem J* **474**, 3355-3371 (2017).
778 7. Liu, X. *et al.* Reversible phosphorylation of Rpn1 regulates 26S proteasome assembly
779 and function. *Proc Natl Acad Sci U S A* **117**, 328-336 (2020).
780 8. Duan, J. *et al.* Conserved Mitotic Phosphorylation of a Proteasome Subunit Regulates
781 Cell Proliferation. *Cells* **10**(2021).
782 9. Zhang, X. *et al.* DNA damage-induced proteasome phosphorylation controls substrate
783 recognition and facilitates DNA repair. *Proc Natl Acad Sci U S A* **121**, e2321204121
784 (2024).
785 10. Basu, S., Greenwood, J., Jones, A.W. & Nurse, P. Core control principles of the
786 eukaryotic cell cycle. *Nature* **607**, 381-386 (2022).
787 11. Suski, J.M. *et al.* CDC7-independent G1/S transition revealed by targeted protein
788 degradation. *Nature* **605**, 357-365 (2022).
789 12. Zheng, X.F. *et al.* CDK5-cyclin B1 regulates mitotic fidelity. *Nature* **633**, 932-940
790 (2024).
791 13. Liu, Y. *et al.* Expanded diversity of Asgard archaea and their relationships with

792 eukaryotes. *Nature* **593**, 553-557 (2021).

793 14. Koonin, E.V. & Yutin, N. The Dispersed Archaeal Eukaryome and the Complex
794 Archaeal Ancestor of Eukaryotes. *Cold Spring Harbor Perspectives in Biology*
795 **6**(2014).

796 15. Spang, A., Caceres, E.F. & Ettema, T.J.G. Genomic exploration of the diversity,
797 ecology, and evolution of the archaeal domain of life. *Science* **357**(2017).

798 16. Samson, R.Y., Obita, T., Freund, S.M., Williams, R.L. & Bell, S.D. A role for the
799 ESCRT system in cell division in archaea. *Science* **322**, 1710-3 (2008).

800 17. Samson, R.Y. *et al.* Molecular and structural basis of ESCRT-III recruitment to
801 membranes during archaeal cell division. *Mol Cell* **41**, 186-96 (2011).

802 18. Liu, J. *et al.* Functional assignment of multiple ESCRT-III homologs in cell division and
803 budding in Sulfolobus islandicus. *Mol Microbiol* **105**, 540-553 (2017).

804 19. Liu, J.F. *et al.* A relay race of ESCRT-III paralogs drives cell division in a
805 hyperthermophilic archaeon. *Mbio* **16**(2025).

806 20. Lundgren, M., Andersson, A., Chen, L.M., Nilsson, P. & Bernander, R. Three
807 replication origins in Sulfolobus species: Synchronous initiation of chromosome
808 replication and asynchronous termination. *Proceedings of the National Academy of*
809 *Sciences of the United States of America* **101**, 7046-7051 (2004).

810 21. Robinson, N.P. *et al.* Identification of two origins of replication in the single
811 chromosome of the Archaeon. *Cell* **116**, 25-38 (2004).

812 22. Ishino, Y. & Ishino, S. Rapid progress of DNA replication studies in Archaea, the third
813 domain of life. *Science China-Life Sciences* **55**, 386-403 (2012).

814 23. Duggin, I.G., Dubarry, N. & Bell, S.D. Replication termination and chromosome dimer
815 resolution in the archaeon Sulfolobus solfataricus. *Embo J* **30**, 145-53 (2011).
816 24. Kalliomaa-Sanford, A.K. *et al.* Chromosome segregation in Archaea mediated by a
817 hybrid DNA partition machine. *Proceedings of the National Academy of Sciences of*
818 *the United States of America* **109**, 3754-3759 (2012).
819 25. Blombach, F., Matelska, D., Fouqueau, T., Cackett, G. & Werner, F. Key Concepts
820 and Challenges in Archaeal Transcription. *Journal of Molecular Biology* **431**,
821 4184-4201 (2019).
822 26. Feng, X., Huang, Q.H. & She, Q.X. Crenarchaeal 3D Genome: A Prototypical
823 Chromosome Architecture for Eukaryotes. *Cell* **179**, 56-58 (2019).
824 27. Takemata, N., Samson, R.Y. & Bell, S.D. Physical and Functional
825 Compartmentalization of Archaeal Chromosomes. *Cell* **179**, 165-+ (2019).
826 28. Tarrason Risa, G. *et al.* The proteasome controls ESCRT-III-mediated cell division in
827 an archaeon. *Science* **369**(2020).
828 29. Yang, Y. *et al.* A novel RHH family transcription factor aCcr1 and its viral homologs
829 dictate cell cycle progression in archaea. *Nucleic Acids Res* **51**, 1707-1723 (2023).
830 30. Li, X.Y., Cristina, L.M., Laura, M.A. & Xu, P. A clade of RHH proteins ubiquitous in
831 Sulfolobales and their viruses regulates cell cycle progression. *Nucleic Acids*
832 *Research* **51**, 1724-1739 (2023).
833 31. Maupin-Furlow, J.A., Gil, M.A., Karadzic, I.M., Kirkland, P.A. & Reuter, C.J.
834 Proteasomes: Perspectives from the Archaea. *Frontiers in Bioscience-Landmark* **9**,
835 1743-1758 (2004).

836 32. Anjum, R.S. *et al.* Involvement of a eukaryotic-like ubiquitin-related modifier in the
837 proteasome pathway of the archaeon Sulfolobus acidocaldarius. *Nat Commun* **6**, 8163
838 (2015).
839 33. Zhang, C., Phillips, A.P.R., Wipfler, R.L., Olsen, G.J. & Whitaker, R.J. The essential
840 genome of the crenarchaeal model Sulfolobus islandicus. *Nat Commun* **9**, 4908
841 (2018).
842 34. Kumoi, K. *et al.* An Archaeal Homolog of Proteasome Assembly Factor Functions as a
843 Proteasome Activator. *Plos One* **8**(2013).
844 35. Sikdar, A., Satoh, T., Kawasaki, M. & Kato, K. Crystal structure of archaeal homolog of
845 proteasome-assembly chaperone PbaA. *Biochemical and Biophysical Research*
846 *Communications* **453**, 493-497 (2014).
847 36. Kennelly, P.J. Protein Ser/Thr/Tyr phosphorylation in the Archaea. *J Biol Chem* **289**,
848 9480-7 (2014).
849 37. Manning, G., Whyte, D.B., Martinez, R., Hunter, T. & Sudarsanam, S. The protein
850 kinase complement of the human genome. *Science* **298**, 1912-34 (2002).
851 38. Hanks, S.K. Genomic analysis of the eukaryotic protein kinase superfamily: a
852 perspective. *Genome Biology* **4**(2003).
853 39. Knuppel, R. *et al.* Insights into the evolutionary conserved regulation of Rio ATPase
854 activity. *Nucleic Acids Res* **46**, 1441-1456 (2018).
855 40. Wu, P.J. *et al.* The archaeal KEOPS complex possesses a functional Gon7 homolog
856 and has an essential function independent of the cellular t6A modification level. *mLife*
857 **2**, 11-27 (2023).

858 41. Reimann, J. *et al.* Regulation of archaella expression by the FHA and von Willebrand
859 domain-containing proteins ArnA and ArnB in Sulfolobus acidocaldarius. *Mol Microbiol*
860 **86**, 24-36 (2012).
861 42. Li, L.L. *et al.* Wing phosphorylation is a major functional determinant of the Lrs14-type
862 biofilm and motility regulator AbfR1 in. *Molecular Microbiology* **105**, 777-793 (2017).
863 43. Huang, Q., Lin, Z., Wu, P., Ni, J. & Shen, Y. Phosphoproteomic Analysis Reveals
864 Rio1-Related Protein Phosphorylation Changes in Response to UV Irradiation in
865 Sulfolobus islandicus REY15A. *Front Microbiol* **11**, 586025 (2020).
866 44. Jiang, Z.C. *et al.* The FHA domain protein ArnA functions as a global DNA damage
867 response repressor in the hyperthermophilic archaeon. *Mbio* **14**(2023).
868 45. Huang, Q., Zhong, Q., Mayaka, J.B.A., Ni, J. & Shen, Y. Autophosphorylation and
869 Cross-Phosphorylation of Protein Kinases from the Crenarchaeon Sulfolobus
870 islandicus. *Front Microbiol* **8**, 2173 (2017).
871 46. Lundgren, M. & Bernander, R. Genome-wide transcription map of an archaeal cell
872 cycle. *Proc Natl Acad Sci U S A* **104**, 2939-44 (2007).
873 47. Peng, N. *et al.* A synthetic arabinose-inducible promoter confers high levels of
874 recombinant protein expression in hyperthermophilic archaeon Sulfolobus islandicus.
875 *Appl Environ Microbiol* **78**, 5630-7 (2012).
876 48. Kisselev, A.F. & Goldberg, A. Monitoring activity and inhibition of 26S proteasomes
877 with fluorogenic peptide substrates. *Ubiquitin and Protein Degradation, Part A* **398**,
878 364-378 (2005).
879 49. Rabl, J. *et al.* Mechanism of gate opening in the 20S proteasome by the proteasomal

880 ATPases. *Mol Cell* **30**, 360-8 (2008).

881 50. Yu, Y. *et al.* Interactions of PAN's C-termini with archaeal 20S proteasome and
882 implications for the eukaryotic proteasome-ATPase interactions. *EMBO J* **29**, 692-702
883 (2010).

884 51. Yu, Z. *et al.* Allosteric coupling between alpha-rings of the 20S proteasome. *Nat*
885 *Commun* **11**, 4580 (2020).

886 52. Reimann, J. *et al.* Archaeal Signal Transduction: Impact of Protein Phosphatase
887 Deletions on Cell Size, Motility, and Energy Metabolism in. *Molecular & Cellular*
888 *Proteomics* **12**, 3908-3923 (2013).

889 53. Pulschen, A.A. *et al.* Live Imaging of a Hyperthermophilic Archaeon Reveals Distinct
890 Roles for Two ESCRT-III Homologs in Ensuring a Robust and Symmetric Division.
891 *Current Biology* **30**, 2852-+ (2020).

892 54. Hirano, Y. *et al.* A heterodimeric complex that promotes the assembly of mammalian
893 20S proteasomes. *Nature* **437**, 1381-1385 (2005).

894 55. Le Tallec, B. *et al.* 20S proteasome assembly is orchestrated by two of chaperones in
895 yeast distinct pairs and in mammals. *Molecular Cell* **27**, 660-674 (2007).

896 56. Stadtmueller, B.M. *et al.* Structure of a Proteasome Pba1-Pba2 Complex. *Journal of*
897 *Biological Chemistry* **287**, 37371-37382 (2012).

898 57. Ramos, P.C., Hockendorff, J., Johnson, E.S., Varshavsky, A. & Dohmen, R.J. Ump1p
899 is required for proper maturation of the 20S proteasome and becomes its substrate
900 upon completion of the assembly. *Cell* **92**, 489-499 (1998).

901 58. Li, X., Kusmierczyk, A.R., Wong, P., Emili, A. & Hochstrasser, M. β-subunit

902 appendages promote 20S proteasome assembly by overcoming an Ump1-dependent
903 checkpoint. *Embo Journal* **26**, 2339-2349 (2007).
904 59. Hirano, Y. *et al.* Dissecting β-ring assembly pathway of the mammalian 20S
905 proteasome. *Embo Journal* **27**, 2204-2213 (2008).
906 60. Zhang, H.X., Zhou, C.Y., Mohammad, Z. & Zhao, J.H. Structural basis of human 20S
907 proteasome biogenesis. *Nature Communications* **15**(2024).
908 61. Guo, X. *et al.* Site-specific proteasome phosphorylation controls cell proliferation and
909 tumorigenesis. *Nat Cell Biol* **18**, 202-12 (2016).
910 62. Groves, M.R. & Barford, D. Topological characteristics of helical repeat proteins.
911 *Current Opinion in Structural Biology* **9**, 383-389 (1999).
912 63. Duggin, I.G., McCallum, S.A. & Bell, S.D. Chromosome replication dynamics in the
913 archaeon. *Proceedings of the National Academy of Sciences of the United States of*
914 *America* **105**, 16737-16742 (2008).
915 64. Cammarano, P. *et al.* Insensitivity of Archaebacterial Ribosomes to Protein-Synthesis
916 Inhibitors - Evolutionary Implications. *Embo Journal* **4**, 811-816 (1985).
917 65. Foo S., K.Y., Traparić J., Grogan D. W., Baum B. A temperature sensitive mutant
918 screen reveals translational stress-induced cell cycle regulation in a thermophilic
919 archaeon. *biorixv preprint* (2025).
920 66. Li, Y. *et al.* Harnessing Type I and Type III CRISPR-Cas systems for genome editing.
921 *Nucleic Acids Res* **44**, e34 (2016).
922 67. Schleper, C., Kubo, K. & Zillig, W. The particle SSV1 from the extremely thermophilic
923 archaeon Sulfolobus is a virus: demonstration of infectivity and of transfection with

924 viral DNA. *Proc Natl Acad Sci U S A* **89**, 7645-9 (1992).

925 68. Schmittgen, T.D. & Livak, K.J. Analyzing real-time PCR data by the comparative C(T)

926 method. *Nat Protoc* **3**, 1101-8 (2008).

927 69. Wisniewski, J.R., Zougman, A., Nagaraj, N. & Mann, M. Universal sample preparation

928 method for proteome analysis. *Nature Methods* **6**, 359-U60 (2009).

929

930

Table 1. Identification of phosphorylated residues in PsmA in the phosphorproteome analysis of ePK2 overexpression strain

Position of PsmA	Motif [a]	pSeSD	pSeSD-ePK2	Fold Change
T213	EKLTPNTVEIGYA	149271.2	1743609.1	11.68081
S200	LALKALSATLKPN	525092.97	1404456.6	2.674682
S59	EKRKAQSLLDVDS	582475.81	555168.13	0.953118
S46	IGIKSKSGVVIAS	884005.76	415292.04	0.469784

[a], the phosphorylated sites are indicated in red.

Figures

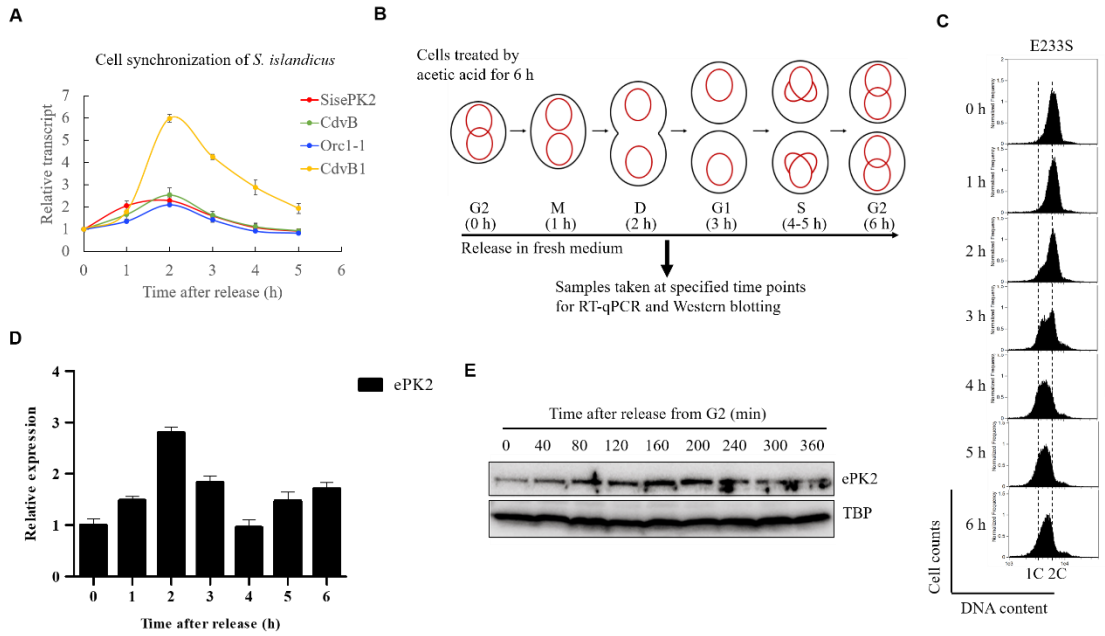

Figure 1. ePK2 exhibits cyclical expression. (**A**) Transcriptional pattern of ePK2 in the cell released from G2 phase. Data obtained from the transcriptomic analysis on synchronized samples of *Sa. islandicus* E233S (Yang *et al*., *Nucleic Acids Res*, 2023) show relative transcription levels of genes encoding for ePK2, DNA replication initiation factor Orc1-1, and two cell division proteins CdvB and CdvB1. Relative transcripts were calculated as FPKM (Fragments Per Kilobase transcript per Million mapped reads) of each gene divided by the level at 0 h, which was set as 1. Error bars represent standard deviations. (**B**) Schematic of the experimental workflow for cell cycle synchronization and time-point sampling of E233S cells. Cells were synchronized with acetic acid treatment for 6 h and released by washing with 20 mM sucrose and culturing in fresh preheated medium. Cells were collected at specified time points after release and total RNA was isolated for RT-qPCR and Western blotting. (**C**) Flow cytometry profiles of *Sa. islandicus* E233S after synchronization. At least 20,000 cells per sample were collected for the analysis. Dashed lines denote cells containing one and two copies of chromosome, 1C and 2C, respectively. (**D**) RT-qPCR verification of the cyclical transcriptional pattern of *ePK2* after synchronization. Data were normalized to 16S rRNA levels. Error bars represent standard derivations of three replicates. (**E**) Western blotting to detect ePK2 in the cells released from G2 phase. Samples at specified time points were analyzed by SDS-PAGE followed by Western blotting with protein-specific antibodies. TBP was used as a reference.

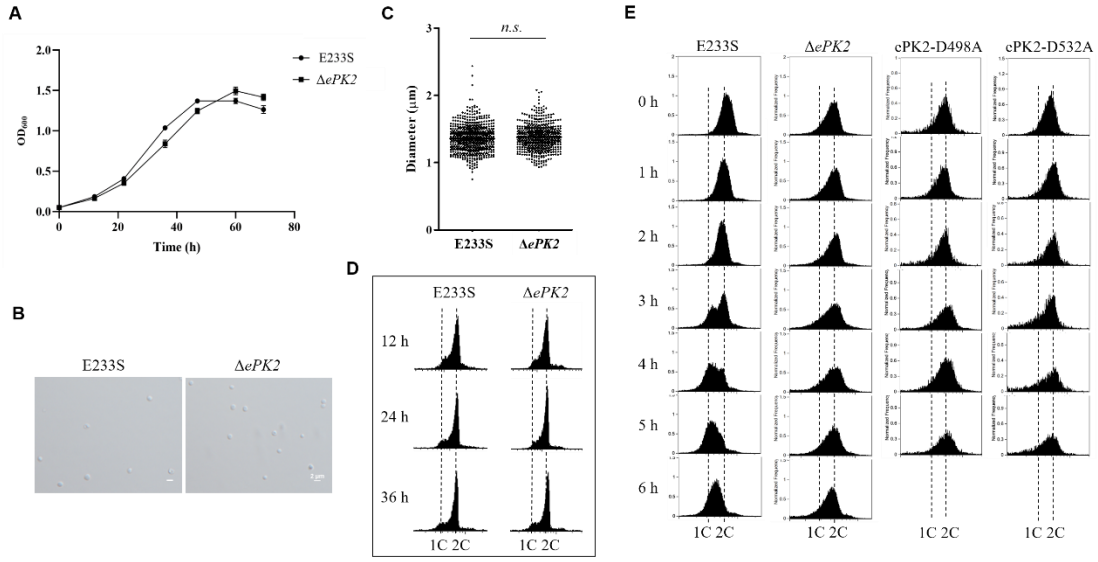

Figure 2. Deletion of *ePK2* impairs cell cycle progression of synchronized cells. (**A**) Growth curves of ΔePK2. Cells were cultured aerobically at 75°C to OD_{600}=0.4-0.8, and then transferred to fresh medium with an initial estimated OD_{600} of 0.05 for follow-up growth curve determination. (**B**) Microscopic analysis of Δ*ePK2*. Samples were taken at early log phase (OD_{600}~0.3) and observed under a NIKON TI-E inverted fluorescence microscope. Scale bar, 2 μm. (**C**) Statistics of cell sizes in (B). Counted number (n) and average diameter (d) for each sample are as follows: E233S (n=579, d=1.366 ± 0.207) and Δ*ePK2* (n=519, d=1.378 ± 0.195). The values (mean ± SD) were obtained based on three independent biological repeats. Significance (*P* value) was calculated by the Wilcoxon test (two-tailed) using GraphPad. *n.s.*, not significant. (**D**) Flow cytometry analysis of *ΔePK2* cells grown at 12 h, 24 h, and 36 h in (A). Samples were fixed by 70% ethanol overnight, washed with PBS buffer and stained with SuperGreen for DNA content analysis. At least 20, 000 cells were analyzed for each sample with over 90% cells from each sample included in the analysis. Dashed lines denote cells containing one and two copies of chromosome, 1C and 2 C, respectively. (**E**) Flow cytometry analysis of *ΔePK2*, ePK2-D498A, and ePK2-D532A after synchronization by acetic acid treatment. Samples were taken at specified time points after released from G2 phase, fixed by 70 % ethanol and stained with propidium iodide (PI) for the analysis.

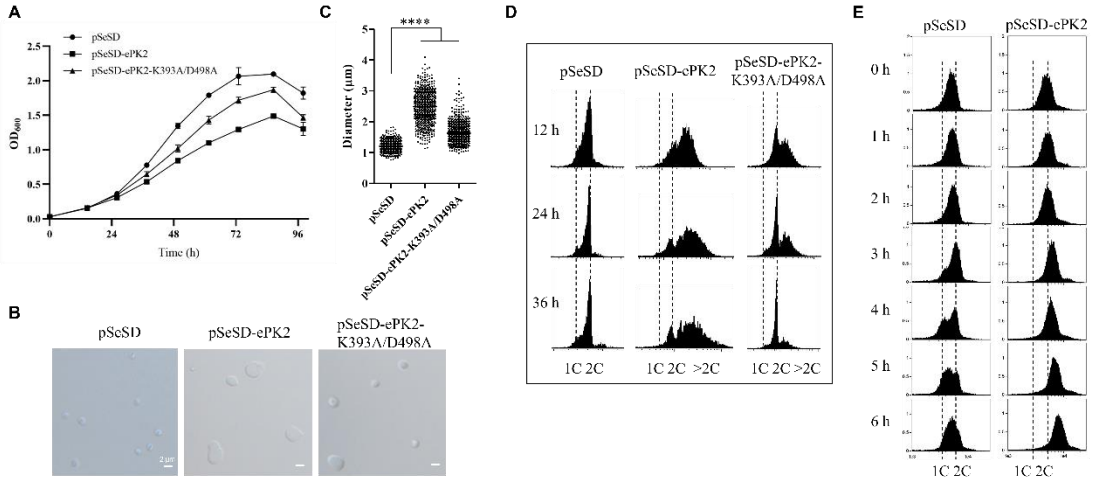

Figure 3. Overexpression of ePK2 hinders cell growth and cell division, resulting in the formation of enlarged cells. (**A**) Growth curves of strains overexpressing ePK2 and its kinase-dead mutants. Protein induction was carried out in ATV medium using pSeSD-based vectors. E233S with the empty vector pSeSD was used as a control. (**B**) Microscopic analysis of strains overexpressing ePK2 and its mutants. Samples were taken at early log phase for microscopy. Scale bar, 2 μm. (**C**) Statistical analysis of cell sizes in (B). Cells carrying pSeSD (n=530, d=1.209 ± 0.173 μm), pSeSD-ePK2 (n=551, d=2.460 ± 0.528 μm) and pSeSD-ePK2-K393A/D498A (n=511, d=1.680 ± 0.370 μm) were analyzed. The values represent the mean ± SD from three independent biological repeats. Significance (*P* value) was calculated using the Wilcoxon test (two-tailed) in GraphPad. ****, $p<0.0001$. (**D**) Flow cytometry of strains overexpressing ePK2 and its mutants. Samples were taken at 12, 24, and 36 h after being cultured in ATV medium. (**E**) Flow cytometry of the ePK2 overexpression strain after release from G2 phase. Cells were synchronized with acetic acid treatment for 6 h, followed by washing out the acetic acid and culturing the cells in ATV medium. The samples were taken at specified time points for flow cytometry analysis with at least 20, 000 cells per sample.

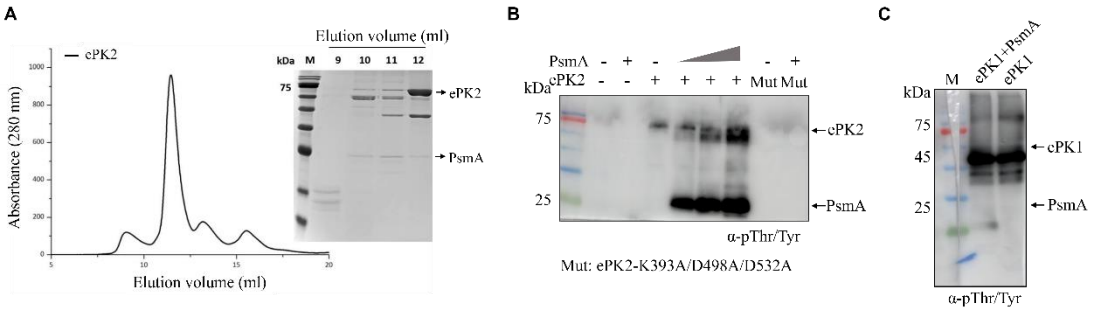

Figure 4. The α subunit of proteasome, PsmA, is a substrate of ePK2. (**A**) Purification of ePK2 from its overexpression strain. Cells were cultured in STV medium for low induction and His-tagged ePK2 was purified with Ni-NTA and gel filtration. The elution profile and SDS-PAGE analysis are shown with bands of ePK2 and PsmA indicated. (**B**) *In vitro* phosphorylation of PsmA by ePK2 and its kinase-dead mutant (Mut). Different concentrations of PsmA (1, 2 and 5 μM) were incubated with 0.5 μM ePK2 or ePK2-Mut (with 5 μm PsmA) at 65°C for 30 min and analyzed by Western blotting using the phosphorylated Thr/Tyr antibody. (**C**) ePK1 phosphorylates PsmA with lower activity compared to ePK2. ePK1 was mixed with 1 μM PsmA and incubated at 65°C for 30 min.

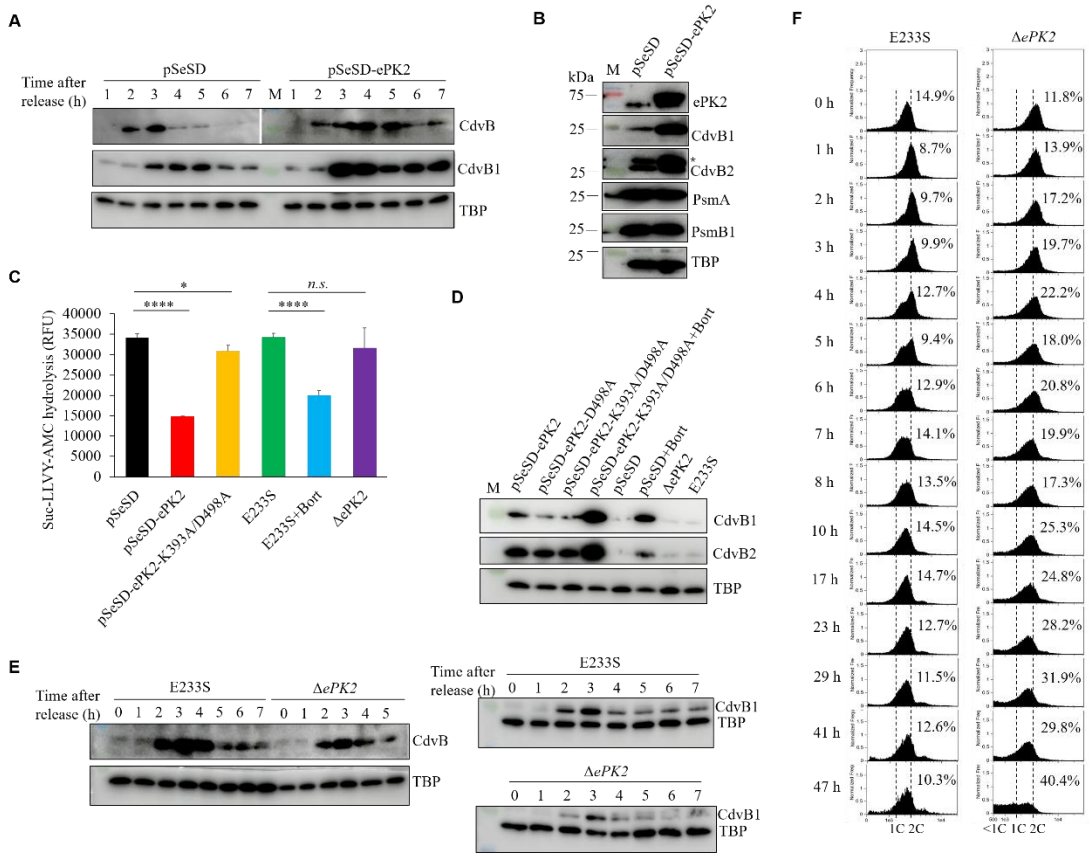

Figure 5. Overexpression of ePK2 inhibits proteasome activity while its deletion stimulates the activity *in vivo*. (**A**) Impaired degradation of CdvB and CdvB1 in synchronized ePK2 overexpression strain. Samples were taken after the cells were released from G2 phase and subjected to Western blot analysis using specific antibodies. (**B**) Accumulation of cell division proteins after ePK2 overexpression. Samples were taken at early log phase. The asterisk indicates the position of CdvB2. (**C**) Decreased *in vivo* proteasome activity in asynchronized cells with ePK2 overexpression but not *ePK2* deletion. Proteasome activities of whole cell lysate (WCL) of ePK2 overexpression and deletion strains were measured using the fluorescent oligopeptide Suc-LLVY-AMC as the substrate. The reaction mixture was incubated at 70°C for 30 min and detected by microplate spectrometer. E233S WCL treated with the proteasome specific inhibitor Bortezomib was served as a positive control. Significance (*P* value) was determined using a one-tailed *t* test in GraphPad. ****, $p<0.0001$; *n.s.*, no significant. (**D**) Inhibition of CdvB1 and CdvB2 degradation of cells with ePK2 overexpression but not *ePK2* deletion. pSeSD based vectors were used for protein overexpression, with ePK2-D498A and ePK2-K393A/D498A being catalytic dead mutants. (**E**) Enhancement of CdvB and CdvB1 degradation in synchronized *ΔePK2* cells. (**F**) Cell death (<1C) observed in synchronized *ΔePK2* cells after prolonged cultivation. Synchronized cells of E233S and *ΔePK2* were cultivated for 2 days after release from G2 phase and analyzed using flow cytometry. The numbers indicate the percentages of DNA-less cells (<1C).

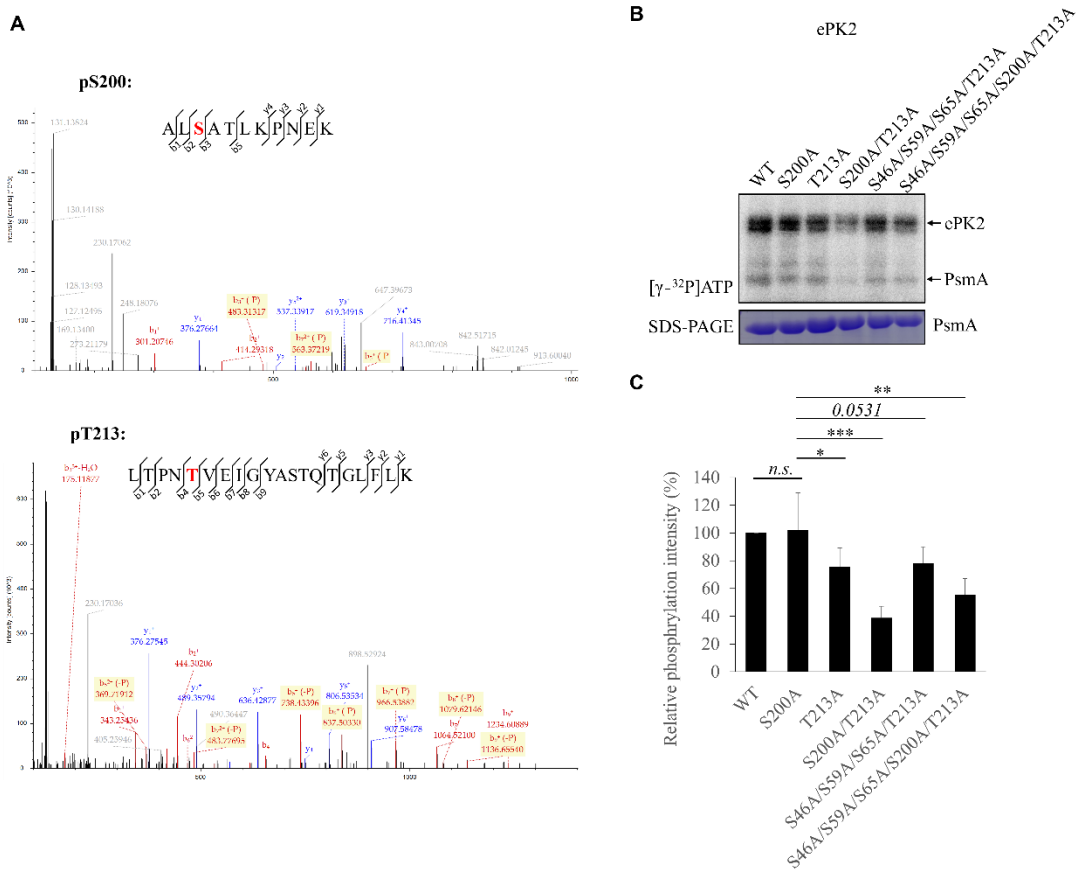

Figure 6. ePK2 phosphorylates PsmA at S200 and T213. (**A**) Mass spectra of two oligopeptides containing phosphorylated S200 and T213. The phosphorylated residues are indicated in red. (**B**) ePK2 phosphorylation on PsmA and its point mutants. The *in vitro* kinase reaction was performed as that in Figure 4B except that [γ-^{32}P]ATP was used instead of cold ATP. Upper panel, radiolabeled exposure of [γ-^{32}P]ATP signal; low panel, SDS-PAGE of PsmA and its mutants. A representative gel is shown. (**C**) Quantitative results of (B). The data show relative phosphorylated ratios between the mutant and wild type (WT) PsmA proteins based on five independent experiments. Significance (*P* value) was calculated using a one-tailed *t* test in GraphPad. *, $p<0.05$; **, $p<0.01$; ***, $p<0.001$; *n.s.*, not significant.

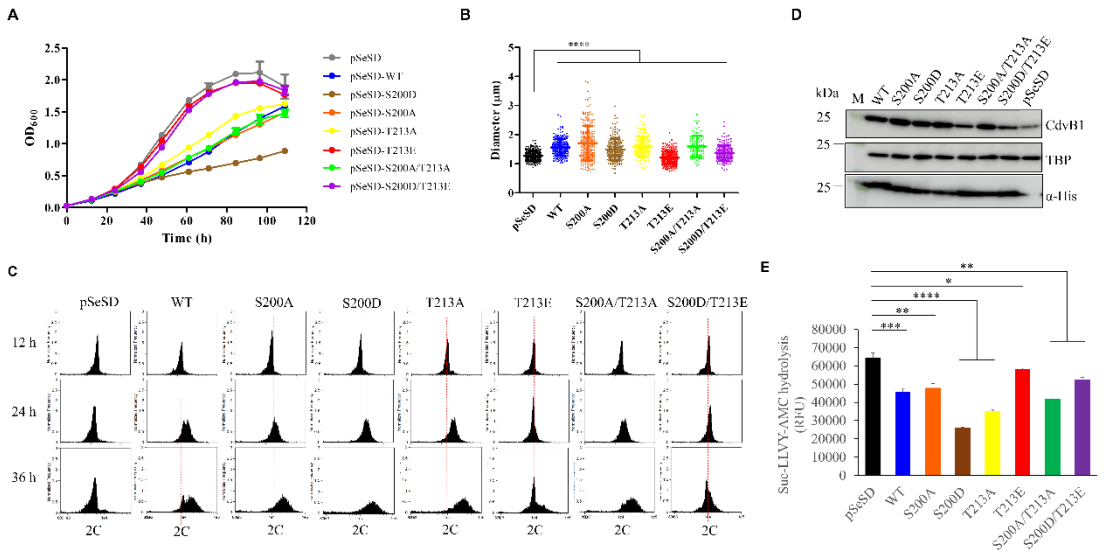

Figure 7. Overexpression of PsmA phospho-mimic mutants S200D and T213E confers different effects on the cell. (**A**) Growth curves of PsmA and its mutant overexpression strains. Cells were cultured in STV medium for 3 times before inoculation in ATV medium to OD_{600}~0.03 for protein induction. (**B**) Statistical analysis of cell sizes of PsmA and its mutant overexpression strains. Cell number counted (n) and average diameter (d) for each strain are as follows: pSeSD (n=280, d=1.274 ± 0.155 μm), WT (n=198, d=1.560 ± 0.287 μm), S200A (n=206, d=1.706 ± 0.599 μm), S200D (n=197, d=1.490 ± 0.370 μm), T213A (n=172, d=1.587 ± 0.356 μm), T213E (n=315, d=1.211 ± 0.206 μm), S200A/T213A (n=97, d=1.596 ± 0.376 μm) and S200D/T213E (n=196, d=1.366 ± 0.258 μm). The values represent the mean ± SD from three independent biological repeats. Significance (*P* value) was calculated using the Wilcoxon test (two-tailed) in GraphPad. ****, $p<0.0001$. (**C**) Flow cytometry profiles of PsmA and its mutant overexpression strains. Cells were cultured in ATV medium and taken at specified time points for flow cytometry. At least 20, 000 cells per sample were analyzed. (**D**) Detection of CdvB1 levels in the overexpression strains of PsmA and its mutants. CdvB1 and PsmA proteins were detected by CdvB1 antibody and a His-tag antibody, respectively, with TBP as a control. (**E**) The proteasome activities of PsmA and its mutant overexpression strains. Significance (*P* value) was determined by the *t* test (one-tailed) using GraphPad. *, $p<0.05$; **, $p<0.01$; ***, $p<0.001$; ****, $p<0.0001$.

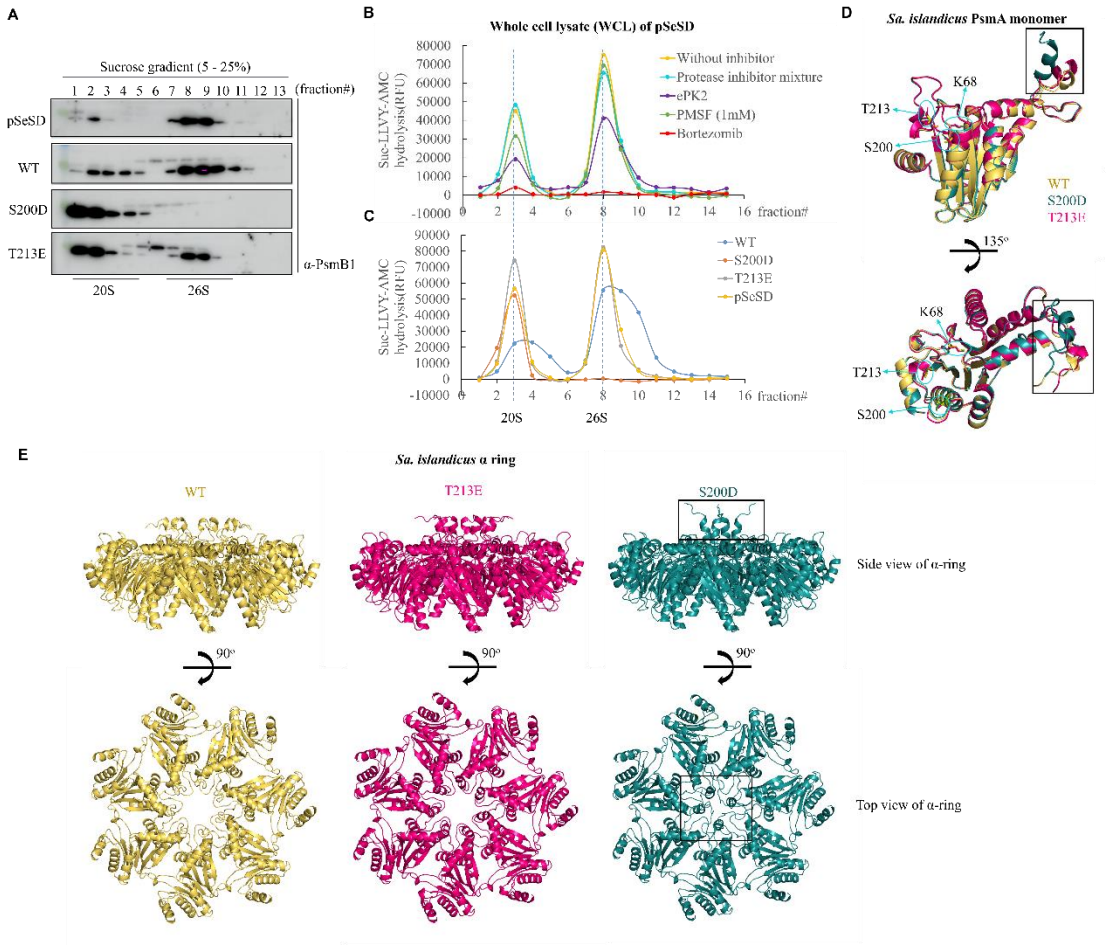

Figure 8. Overexpression of S200D eliminates 26S assembly, while overexpression of T213E has no effect on cellular 20S or 26S assembly (**A**) The isolation of the 20S and 26S proteasomes from cells overexpressing PsmA. A 0.5 ml aliquot of soluble whole cell lysate (WCL) of PsmA overexpression strains was centrifuged with sucrose gradients ranging from 5%–25%. Samples were collected at 1 ml intervals and analyzed by Western blotting with PsmB1 antibody. The positions of 20S and 26S proteasomes are indicated at the bottom of the figure. (**B**) Proteasome activities of WCLs from cells carrying pSeSD and pSeSD-ePK2 with or without inhibitors. (**C**) Proteasome activities of WCLs from pSeSD-PsmA (WT), S200D and T213E. The positions of 20S and 26S proteasomes are indicated at the bottom of the curves. (**D**) Superposition of PsmA (WT) (yellow), S200D (cyan), and T213E (pink) monomers. The structures were predicted by AlphaFold 3. Phosphorylated residues, S200 and T213, and the conserved K68 interacting with HbYX motif are indicated by circles. The black rectangle highlights the conformational change in S200D. (**E**) Comparison of WT (yellow), S200D (cyan), and T213E (pink) heptamer rings. The upper panel shows a side view and the lower panel shows a top view, with black rectangles indicating conformational changes of S200D within the α ring.

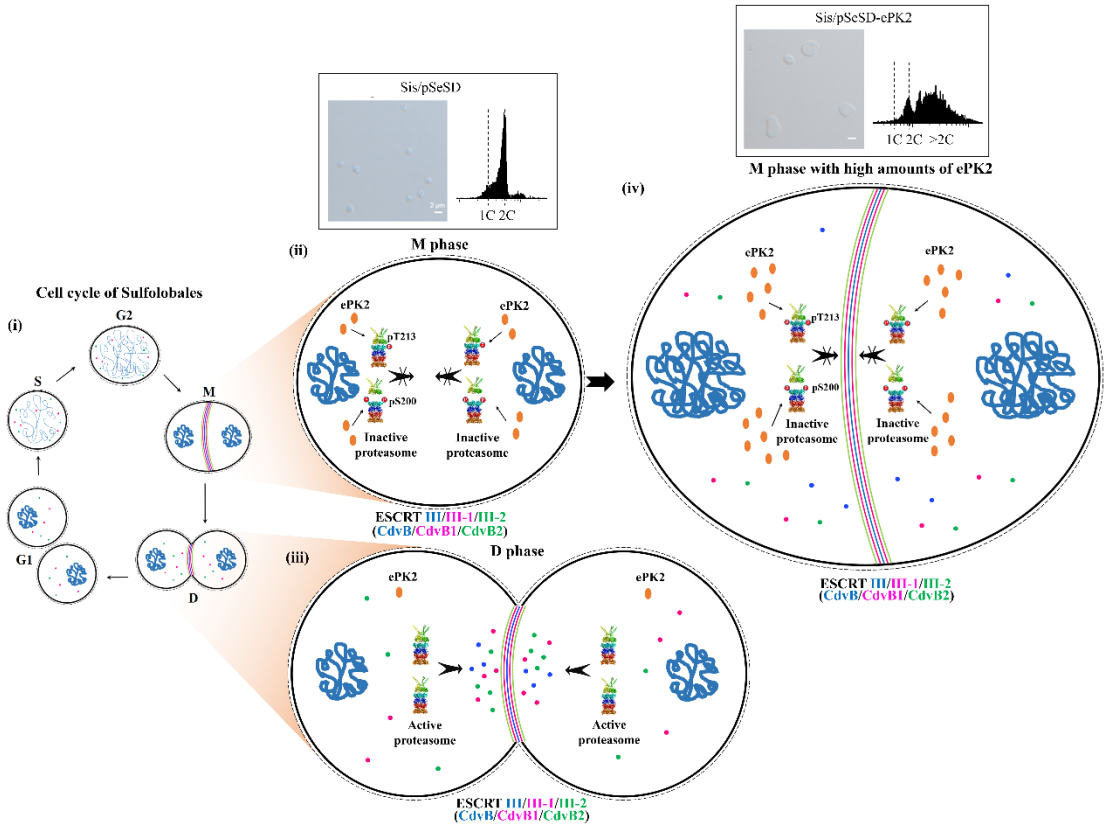

Figure 9. A proposed model of cell division regulation by ePK2 phosphorylation of the proteasome in Sulfolobales. (**i**) The cell cycle of Sulfolobales consists of G1, S, G2, M and D phases. (**ii**) Following the G2 phase, an increase in ePK2 expression leads to elevated PsmA phosphorylation. This results in the failure of 26S proteasome assembly (S200 phosphorylation) or the formation of inactive 26S proteasome (T213 phosphorylation). Inhibition of proteasome assembly halts the degradation of cell division proteins CdvB/CdvB1/CdvB2, allowing them to accumulate at the mid-cell. (**iii**) During the D phase, the expression of ePK2 decreases, facilitating the assembly and activation of proteasomes for the degradation of CdvB proteins. The reduced transcription of *cdvB* genes by aCcr1 (Yang *et al*., 2023) further stimulates the disassembly of CdvBs rings. This allows the cell cycle to progress with ring constriction and ultimately membrane abscission. (**iv**) When ePK2 is overproduced during M phase, the proteasome remains constantly inhibited, leading to the accumulation of CdvB proteins. This results in enlarged cells with increased DNA contents.